Case Studies in Construction Materials 19 (2023) e02287

Contents lists available at ScienceDirect

Case Studies in Construction Materials

journal homepage: www.elsevier.com/locate/cscm

Case study

Phase transformation and microstructure of in-situ concrete after 20-year exposure to harsh mining environment: A case study

Fulin Qu [a], Hanbing Zhao [a], Kai Wu [b], Yang Liu [c], Xinyu Zhao [d], Wengui Li [a,*]

[a] School of Civil and Environmental Engineering, University of Technology Sydney, NSW 2007, Australia
[b] Department of Civil Engineering, Monash University, Clayton, VIC 3800, Australia
[c] YAT Construction and Engineering, Perth, WA 6000, Australia
[d] State Key Laboratory of Subtropical Building Science, South China University of Technology, Guangdong 510641, China

ARTICLE INFO

Keywords:
Concrete
Deterioration
Mining environment
Chloride ingress
Chemical reaction
Micro characterization

ABSTRACT

The phase transformations and microstructural properties of a drilled cylinder specimen from a C40 concrete dam used for mining wastewater disposal were evaluated in this study, covering a span of up to 20 years. Various analysis methods, including PT, ICP-MS, XRD, FTIR, TGA, MIP, and SEM-EDS, were employed to assess the performance of powder samples obtained through layer-by-layer grinding. The results obtained from XRD, FTIR, and TGA analyses indicated that the presence of calcite in all ground powder samples, suggesting that carbonation can occur in all layers, even including the inner layers. Moreover, the MIP and SEM-EDS results illustrated that the microstructural properties of the concrete could be influenced by phase transformations induced by various ions present in the mining wastewater, resulting in increased porosity and looser interfacial transition zones (ITZs) in the sample closer to the outer layer. The PT results confirmed the penetration of chloride into the concrete, although the relative chloride content decreased with the increasing depth of the layers. It was observed through TGA analysis that a portion of the chloride ions could attribute to the formation of Friedel's salts, derived from ettringite or calcium aluminate monosulfate. Additionally, SEM-EDS examination revealed that some chloride ions could bind to the C-S-H gels. The presence of different ions, particularly magnesium ions in the mining wastewater could lead to decalcification of the hydrated gels. These research findings provide significant support for the safety assessment of the concrete structure exposed to mining environments.

1. Introduction

Concrete is a versatile, low-cost, and highly durable building material that typically does not require maintenance throughout the entire service life of a structure. However, the performance of concrete can be deteriorated by a few chemical reactions between the

Abbreviations: AFm, Calcium aluminate monosulfate; AFt, Ettringite; CH, Portlandite; C_3A, Tri-calcium aluminate; C-S-H, Calcium silicate hydrate; DMW, Dam reservoirs wastewater; DTG, Differential thermogravimetric; FTIR, Fourier transform infrared spectroscopy; FS, Friedel's salts; G, Gypsum; GGBFS, Ground granulated blast-furnace slag; ITZs, Interfacial transition zones; ICP-MS, Inductively coupled plasma mass spectrometry; MDW, Mine drain wastewater; MIP, Mercury intrusion porosimetry; M-S-H, Magnesium silicate hydrate; PT, Potentiometric titrator; SEM-EDS, Scanning electron microscopy with energy dispersive X-ray; TG, Thermogravimetric; TGA, Thermogravimetric analysis; XRD, X-ray diffraction.

* Corresponding author.
E-mail address: Wengui.Li@uts.edu.au (W. Li).

https://doi.org/10.1016/j.cscm.2023.e02287
Received 1 May 2023; Received in revised form 16 June 2023; Accepted 5 July 2023
Available online 6 July 2023
2214-5095/© 2023 The Authors. Published by Elsevier Ltd. This is an open access article under the CC BY-NC-ND license (http://creativecommons.org/licenses/by-nc-nd/4.0/).

cement matrices and external environments, like seawater environment, acid underground environment, and aggressive mining environments, etc. [1–4]. In particular, Australia, one of the largest exporters of minerals in the world, has numerous mining companies in the field, where concrete is also the most commonly used building material for mining structures and related protective structures [5,6]. Additionally, the presence of large amounts of unfavorable ions, such as sulfate, chloride, carbonate, or magnesium ions in mining wastewater, can significantly damage the properties of concrete structures, leading to unreliable structural safety and an increased risk of damage to the health and economic well-being of workers. Therefore, it is crucial to have a thorough understanding of the chemical reactions between hydrated products and unfavorable ions in mining environments.

Over the past few decades, numerous research programs have been conducted to investigate the effects of various chemicals on the phase changes and/or microstructure of concrete structures [7–11]. These studies have revealed that certain hydrated products in cement matrices are highly susceptible to interactions with external ions. When concrete structures are exposed to environments with high levels of sulfate ions, certain hydrated products can be greatly affected by chemical reactions. It is generally accepted that the hydrated products usually involve the reaction of sulfate ions with portlandite (CH) and/or some other phases containing aluminas, like tri-calcium aluminate (C_3A), and calcium aluminate monosulfate (AFm), calcium silicate hydrate (C-S-H) gels, etc., which results in the secondary formation of ettringite (AFt), gypsum (G) and/or mannite and thaumasite in specific cases [12–15]. The precipitation of these products, mainly AFt, leads to an increase in solid volume, which is traditionally believed to be the cause of expansion and applied pressure within the matrix, resulting in subsequent material cracking, spalling, and loss of strength [16–18]. Furthermore, some researchers have suggested that when reinforced concrete is exposed to a chloride-rich environment, the concrete binders are rarely affected by the chlorides. However, as the chloride concentration reaches a critical level, the reinforcing steel can become corroded, which can result in a reduction in the overall performance of the concrete structure [19–21]. Chlorides can only penetrate the reinforced steel when they reach a critical level and breach the protective layers. It has been suggested that chlorides can react with certain phases in the binder, leading to the secondary formation of calcium chloroaluminate hydrates such as Friedel's salts (FS) or Kuzel's salts. Additionally, chlorides can also be adsorbed onto C-S-H gels. [22–24]. Other chlorides that are present in the pore solution can be transported, which can increase the chloride concentration around the reinforcing steel [25]. Generally, the presence of high concentrations of sulfate and chloride ions in mining wastewater can lead to various chemical reactions with the hydrated products in concrete structures, causing deterioration of the concrete's properties and potentially compromising its structural integrity over time. This highlights the importance of understanding and managing the effects of various ions on concrete structures in mining environments.

Meanwhile, other contained ions in the mining environment, such as magnesium, can also trigger chemical reactions between the hydrated products and the external ions [26]. Magnesium ions can react with CH, leading to the precipitation of brucite. It is also reported that magnesium ions can exchange with the calcium ions present in C-S-H gels, causing the formation of magnesium silicate hydrate (M-S-H) gels, which can lead to unstable microstructures in the concrete matrices [27–29]. Additionally, carbonate ions may exist in various forms in the solution, such as CO_3^{2-} ($pH \leq 9$) or HCO_3^- ($6 \leq pH < 9$), and they may react with CH, leading to the formation of calcite [30–32]. This carbonation process can lead to a decrease in the pH of the concrete pore solution, which can cause the passive layer on the reinforcing steel to become unstable. Besides, the presence of calcite and magnesium ions can also trigger the transformation of C-S-H gels into thaumasite, a non-cementitious product that can cause the disintegration of the concrete structure [33–35]. The individual and combined effects of aggressive ions mentioned above can lead to significant damage to concrete structures in mining environments, compromising their structural safety and service life. It is therefore important to carefully consider the chemical reactions and potential sources of aggressive ions when designing and constructing concrete structures in mining environments [36,37].

However, it should be emphasized that the information and many of the specifics mentioned above were obtained from laboratory-based experimental research. While the actual situation in the field is significantly more complex, experimental studies in the lab have the advantage of being able to carefully regulate the test settings. Ideally, the results obtained from these experiments can serve as a basis for understanding the fundamental mechanisms underlying the chemical reactions between aggressive ions and concrete structures, and for developing strategies to mitigate their adverse effects in practical applications [7]. Besides, it is important to conduct further research and field studies to validate the laboratory findings and to develop more accurate models that can account for the effects of multiple interacting factors in real-world conditions [38–40]. Therefore, in light of the aforementioned limitations of laboratory-based research, this study aimed to investigate the combined chemical attack of various ions present in mining environments on concrete structures using a drilled cylinder specimen from a concrete dam in Western Australia. The dam has been underused for more than 20 years, providing an opportunity to examine the long-term effects of exposure to mining conditions on concrete.

Table 1
Composition of the concrete (kg/m^3).

Cement	231
GGBFS	99 (30 %)
Sand	740
Gravel	1157
Water	149
Air entrainer	0.15
Superplasticizer	1.65

2. Experimental program

2.1. Specimen preparations

In 2002, a concrete dam was constructed and commissioned in Western Australia to collect mining wastewater, which would then be treated by the sewage treatment center. The composition of C40 concrete used in the dam was shown in Table 1. Here, 30 wt % Ground granulated blast-furnace slag (GGBFS) was used to replace the cement in the binder. The pH and ion concentration of two wastewater samples from the mine drain and dam reservoirs were analyzed using a Thermo-pH meter and inductively coupled plasma mass spectrometry (ICP-MS), the results of which are shown in Table 2. As shown in Table 2, the two wastewater samples were found to have relatively high concentrations of both cations and anions. In particular, the concentration of Cl^- and SO_4^{2-} in the dam reservoirs wastewater (DMW) could be as high as 5000 and 148 mg/L, respectively. The concentration of Mg^{2+} and Ca^{2+} is also relatively high in DMW. The pH of mine drain wastewater (MDW) and DMW are 7.4 and 7.7, respectively. This indicated that the concrete structures under the mining environment can be attacked by the high concentration of various salts.

To analyze the degradation of the concrete under the practical mining environment, a cylindrical specimen measuring 63 mm in diameter and approximately 100 mm in height was drilled from the dam's concrete when the wastewater was in a lower level. The sampling process is shown in Fig. 1. No reinforcements were contained in the cylinder concrete sample. After drilling, the cylinder concrete specimen was dried using a clean cloth and subsequently sealed in a plastic bag. The specimen was then stored in a vacuum drying machine at 40 °C until it was analyzed.

Fig. 2 displays the schematic procedure of testing sample preparations from the drilled cylinder specimen. The drilled cylinder specimen was split into two parts along its axis. One part was cut into different layers from the erosion surface as follows: 0–5, 5–10, 10–15, 15–20, 20–30, 30–40, 40–50, and 50–60 mm. Most of the different slice layers samples were ground into a powder with a particle size smaller than 75 μm, and the powder samples were then dried in a vacuum oven at 40 °C before further phase transformation analysis. In particular, the number of dried powder samples in each layer was about 20–40 g. In addition, the left slice layer samples with 2 or 3 mm were adopted by a cutting machine for pore microstructural analysis. For another part, two cubic slice samples with around size of 20 mm in length and width, 5 mm in height were extracted from the middle of the concrete specimen for microstructural analysis. One of the slice samples was taken from the erosion surface, while another was taken from the inner surface. The slice samples were also dried at 40 °C in a vacuum oven prior to the analysis.

2.2. Methodology

2.2.1. Chloride content and pore solutions determination

To determine the chloride ingress and the distribution of the ions in the pore solution, around 10 g of the dried powder sample in different layers was firstly dissolved in 100 ml acidified deionized solution (deionized water: 70 wt % HNO_3 solution) and rotated slowly for 2 h. Then, after heating at 80 °C for 2 h and cooling down to the normal temperature, 20 ml of the dissolved solution was rotated slightly for 2 h and filtrated with a 4 μm cellulose filter. The filtrated solution was adopted for the chloride determination and ICP-MS test. The chloride content of one part of the filtrated solution was measured by the chloride potentiometric titrator (PT), while the concentrations of different elements including Al, Si, Ca, Mg, Na, and K in another filtrated solution were measured by ICP-MS. In particular, the chloride content and concentrations of the various elements determined in the solution were recalculated in relation to the dry mass of the sample (weight after drying at 105 °C) [22].

2.2.2. Mineralogical characterization analysis

To explore the phase transformations of the drilled concrete specimen caused by the mining environment, the dried powder samples were tested by various methods including thermogravimetric analysis (TGA), X-ray diffraction (XRD) and Fourier transform infrared spectroscopy (FTIR). For the TGA test, around 50 mg of the dried powder sample was determined by the NETZSCH STA F3 Jupiter purged with N_2 at 100 ml/min. The dried powder sample was firstly loaded in an alumina crucible, and then heated at 40 °C for 20 min. After that, the heating temperature was increased to 1000 °C at a speed of 10 °C/min. For the XRD test, around 2–3 g of dried powder sample was measured by a Bruker D8 Discover diffractometer with Cu Kα radiation source of wavelength 1.54 Å. The dried powder samples were evenly loaded in a glass plate and determined in the range of 5–70° 2θ at a step of 0.02° for 30 min. For the FTIR test, around 0.5–1 g of dried powder sample was determined by the Nicolet 6700 FTIR spectrometer, and the measurement was performed between 450 and 4000 cm^{-1} wavenumbers at an increment of 8 cm^{-1}.

2.2.3. Microstructural characterization

The dried slice samples with around 10 mm in both width and length were adopted by a cutting machine to do the microstructural

Table 2
Ion concentrations (mg/L) and pH of water samples.

Items	Sr^{2+}	Ca^{2+}	K^+	Mg^{2+}	Na^+	SO_4^{2-}	Si^{4+}	Cl^-	pH
MDW	60	4120	384	1770	13,000	428	12	30,700	7.4
DMW	6.91	519	244	211	2560	148	30	5000	7.7

Note: MDW stands for the wastewater sample from the mine drain; DMW stands for the wastewater sample from the dam reservoirs.

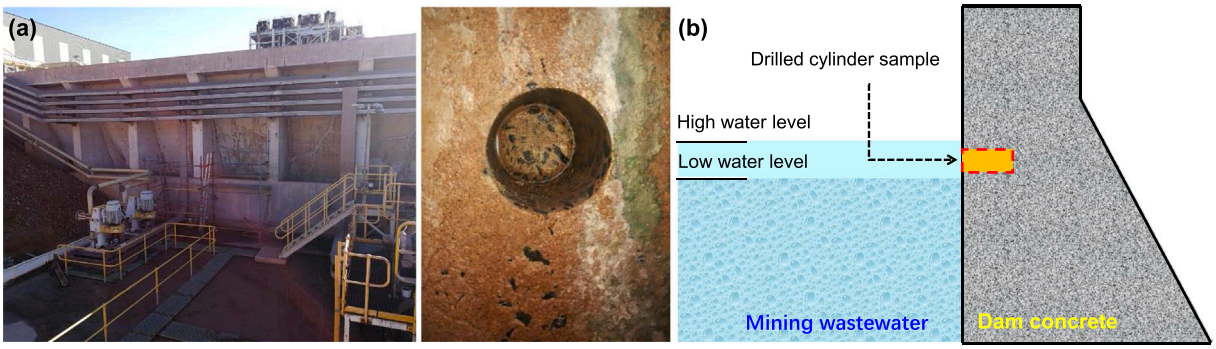

Fig. 1. Concrete sampling process: (a) on-site dam in Western Australia (2022); (b) the cylinder specimen drilled from the concrete dam interacted with the wastewater.

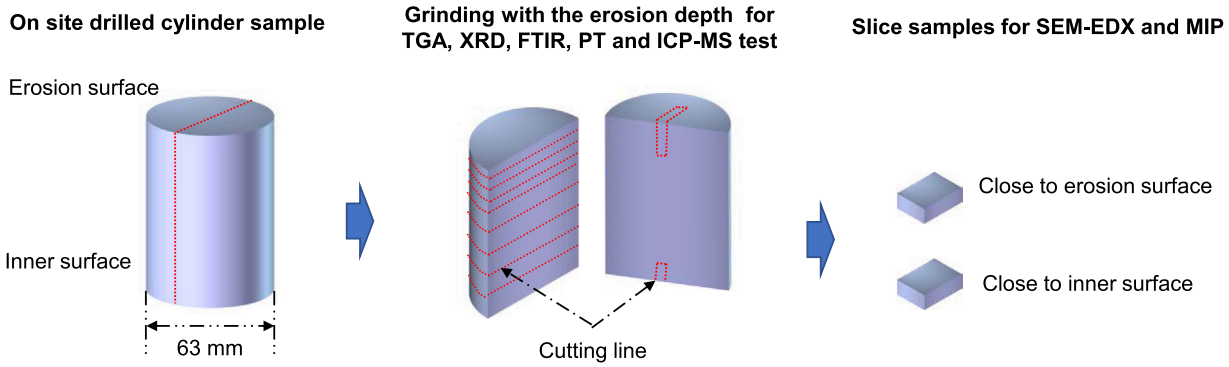

Fig. 2. Sample preparations from the drilled cylinder concrete.

analysis test by using scanning electron microscopy with energy dispersive X-ray (SEM-EDS). The dried slice samples were coated with carbon in the Leica EM ACE600 Sputtering and determined by the Zeiss Supra 55VP SEM at a speed-up voltage of 15 keV and a working distance of around 10 mm. Different element (including Na, C, Mg, Al, Si, Cl, Ca, O, and S) atomic percentages were recorded and analyzed by Aztec version 2.0 software based on EDS results.

2.2.4. Mercury intrusion porosimetry (MIP)

The dried slice samples with around 2–3 mm in both width and length were evaluated with a mercury intrusion porosimeter (Premaster GT-60, Kangta Instrument Company, USA) at a maximum pressure of 210 MPa and contact angle of 140.

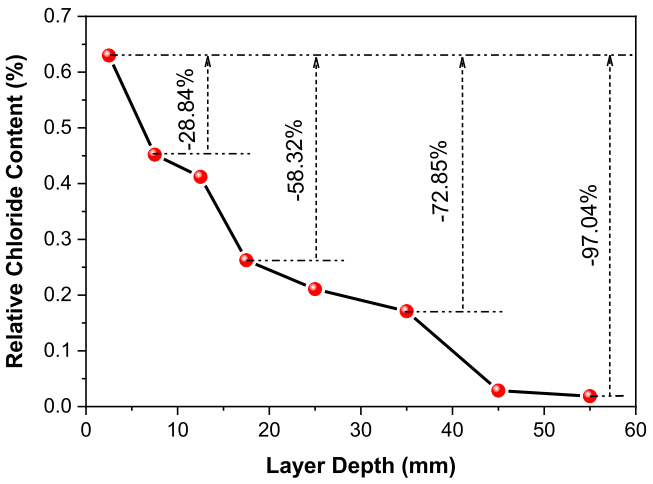

Fig. 3. Relative chloride content of the drilled samples in different layer depths.

3. Results and discussions

3.1. Change in chemical ions

3.1.1. Chloride ingress

Fig. 3 displays the relative chloride content of the drilled sample in different layer depths. The relative chloride content in the drilled sample decreases with the layer depth, and there is virtually no free chloride content in the drilled sample when the layer depth is between 50 and 60 mm, indicating that the chloride ions can penetrate the interior of the drilled cylinder concrete specimen in a relatively high layer depth. Wang et al. [41] and Zhang et al. [42] have mentioned that the transportation of chloride ions is likely related to the transportation of water within the concrete structure, which in turn could be affected by the pore characteristics and the presence of cracks in the concrete matrix. Besides, the varying chloride content at different layers may indicate that the microstructural properties of the concrete can change because of chemical reactions between hydrated products and aggressive ions present in mining environments. The further phase transformations and microstructural properties of the concrete would be examined in the sections.

3.1.2. Pore solution determination

Fig. 4 presents the ICP-MS results of the drilled sample in different layer depths. As mentioned in Section 2, the powder samples in different layers were used for the ICP-MS analysis. Although the fine aggregate in the concrete specimens may have been ground in preparing the powder samples, this study assumes that the changes in the different elements determined by the ICP-MS are attributable to the cement matrices, the assumption of which has also been adopted in some other references [22]. It can be observed that there are noticeable changes in the tested concentrations of all elements from 0 mm to 30 mm depth in all layers, while these changes become less pronounced as the layer depth increases. In the depth range of 0–30 mm, there is a relatively high concentration of Mg, which contributes to the elevated Mg content in the mining solution. Although the mining wastewater contains relatively high levels of Na and K, the maximum concentrations of Na and K detected by ICP-MS are relatively low, which could be attributed to the high binding capacity of Na and K ions by the hydrated gels [43]. Furthermore, the high maximum concentrations of Si and Al near the exposed surface of the concrete might be attributed to the wall effect caused by the rising of the cement matrices and the decreasing presence of larger aggregates. The higher maximum concentration of Ca detected on the outer layer of the drilled samples could be attributed to the formation of calcite resulting from carbonation. The presence of various ions in the mining wastewater, such as magnesium, could increase the leaching of calcium from the pore solution by exchanging calcium ions from hydrated gels, such as C-S-H gels, increasing the maximum concentrations of Ca determined in the ICP-MS [44]. As the layer depth exceeds 30 mm and reaches the inner layers, the minimal changes in the concentrations of different elements may indicate that the various ions in the mining wastewater will have little effect on the hydrated products in the inner layers.

3.2. Change in mineralogical characterizations

3.2.1. X-ray diffraction analysis (XRD)

Fig. 5(a) and (b) display the XRD pattern in different 2 theta ranges for the drilled sample along the layer depth. As seen from Fig. 5 (a), some aluminate-rich hydration phases, including the AFt (2 thetas at 9.1°, PDF#00–041–1451), thaumasite (2 thetas at 9.2°, PDF #00-046-1360). and AFm (2 thetas at 11.6°, PDF #00–41–0063) can be examined in the XRD pattern [45]. There is also a lower peak intensity of AFt and AFm in the outer layers than in the inner layers, which indicates that the phases of AFt and AFm can be converted to other phases, like in the chloride-rich mining environment, the increasing generation of the Friedel's salts [22]. However, there is no

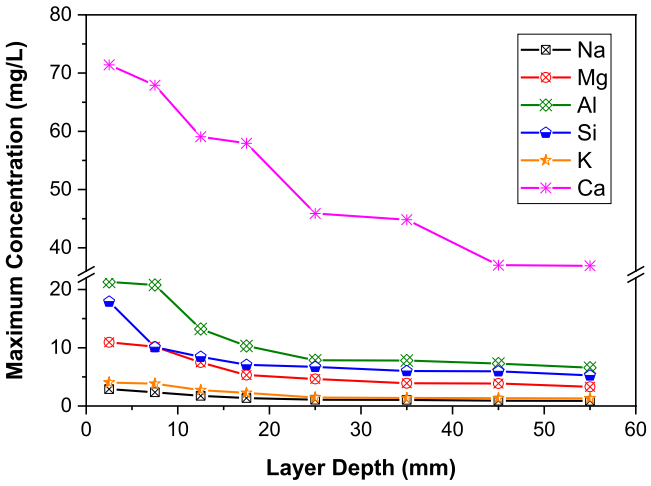

Fig. 4. Maximum concentration of different elements in the drilled sample in different layer depth.

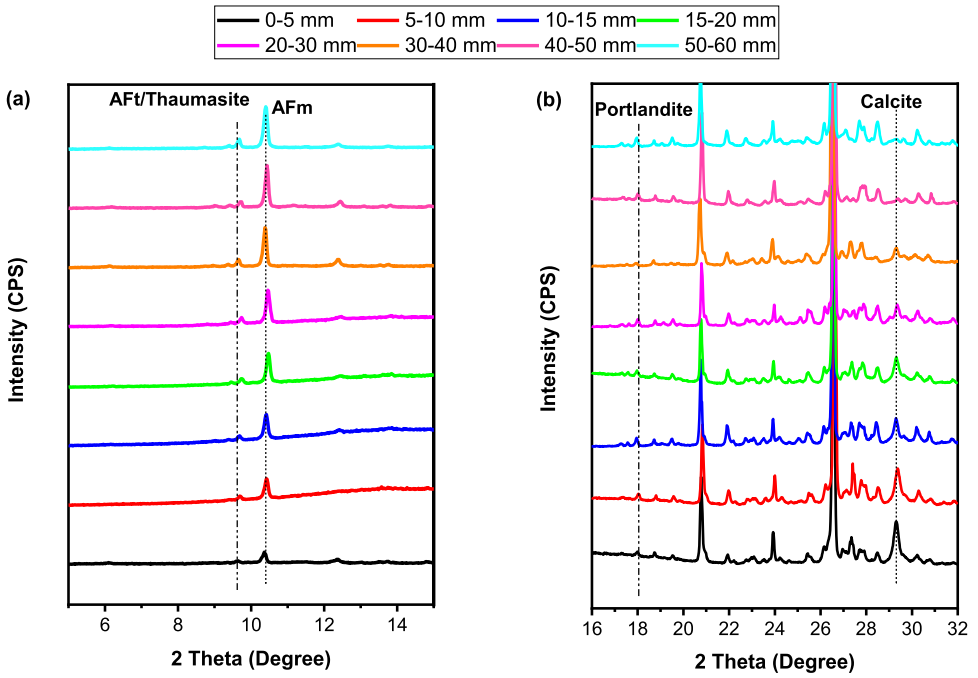

Fig. 5. The XRD pattern of the drilled sample in different layers.

Friedel's salt-related peak in the XRD pattern, which is usually detected in the diffraction peak of 2 theta at around 11.2° (PDF #00–031–0245). This could be attributed to the fact that the powder sample used for testing was prepared by grinding the concrete sample with the aggregate, which might have resulted in the high-intensity peak of quartz that could affect the accuracy of the examination of Friedel's salt in the XRD test [45]. Referring to Fig. 5(b) in a high layer depth, there are two primary alternations of the drilled sample in the different layer depth: one is the peak intensity of portlandite (2 thetas at 18.1°, PDF #00–41–1451); another is the peak intensity of calcite (2 thetas at 29.4°, PDF #00–005–0586). There is a relatively higher intensity of calcite but a lower intensity of portlandite in the outer layers than in the inner layers, which could be attributed to the carbonation reaction between the carbonate ions and the CH [46]. In addition, the presence of calcite in the samples from all layers suggests that carbonation can occur throughout all layers of the concrete, including the deepest layers.

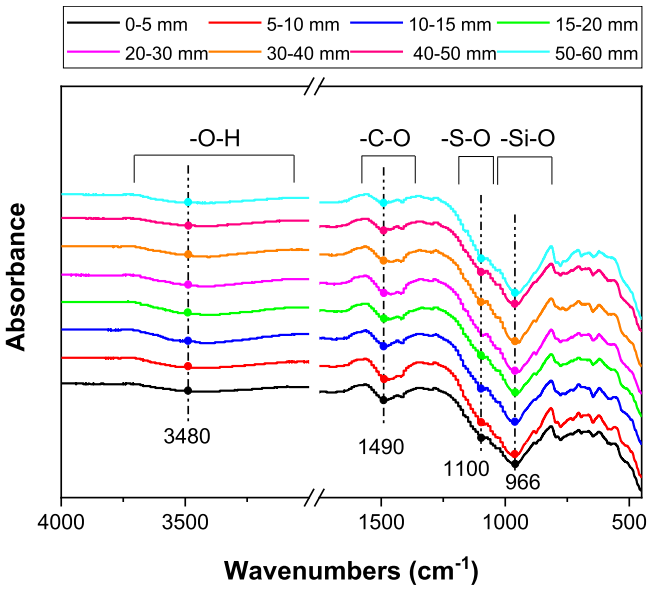

Fig. 6. The FTIR pattern of the drilled sample in different layers.

3.2.2. Fourier transform infrared spectroscopy (FTIR)

Fig. 6 illustrates the FTIR pattern (450–4000 cm^{-1}) of the drilled sample in different layers. It can be examined that there are four primary peaks detected in the FTIR pattern. The largest and most prominent feature at approximately 966 cm^{-1} represents the Si-O stretching in the test sample, which is primarily attributed to the C-S-H gels. The peak variation at 1100 cm^{-1} mainly representatives the S-O bending mode of hydrated phases with S content, including AFt, thaumasite, or AFm. The mode at around 1490 cm^{-1} is mostly contributed to the C-O bending mode of the calcite in the cement matrices. In addition, the mode at 3480 cm^{-1} is mostly due to the -O-H stretching of CH or free water present in the different layers of samples.

The detection of calcite in samples from all layers by FTIR results suggests that carbonation can occur throughout the concrete, which is also supported by the XRD results. Referring to Fig. 6, although the changes in bending modes of S-O, C-O, and -O-H are not apparent in different layer depths in the FTIR results, the changes in corresponding hydrated phases may be determined by other analysis methods such as XRD or TGA. Besides, according to the FTIR results, there appears to be a noticeable variation in the Si-O intensity among samples obtained from different layers. Notably, the intensity of Si-O near the erosion surface is lower than that near the inner surface, which could suggest that the hydrated products, such as the C-S-H gels that may have been deteriorated by external ions present in the mining wastewater.

3.2.3. Thermogravimetric analysis (TGA)

Fig. 7 shows the thermogravimetric (TG) and the differential thermogravimetric (DTG) curves from 40 °C to 1000 °C of the drilled samples in different layers. As could be observed from DTG and TG curves, the dehydration of C-S-H gels, AFt, AFm, CH, and calcite could be detected in all curves at approximately 100–200, 100–120, 160–200, 450–550, and 600–800 °C, respectively. Besides, the DTG and TG curved also showed that the dehydration of Friedel's salts and brucite could also be detected in some curves at around 280–400 °C and 350–450 °C, respectively. It is notable from Fig. 7 that there is a relatively higher mass loss in the hydrated phase of calcite in the sample close to the outer layers than that in the inner layers, which is also corroborated by the XRD and FTIR results mentioned previously. Although no clear peaks of Friedel's salts and brucite were detected in the XRD and FTIR patterns, these phases were detected in the TGA results, suggesting that they could be generated in the samples close to the outer layers. In particular, the mass loss at around 280–400 °C of the samples in the outer layers is higher than that in the inner layers, indicating that chemical reactions between the hydrated phases and the various ions in the mining wastewater can occur after the concrete has been exposed to the mining environment for up to 20 years.

3.3. Change in microstructures

3.3.1. Pore size distribution

Fig. 8(a) and (b) display the pore size distribution and the porosity of the drilled sample in the outer layer (0–5 mm) and the inner layer (50–60 mm), respectively. Based on the pore size distribution results shown in Fig. 8(a), the corresponding porosity for different pore sizes was determined using the critical pore diameter and is listed in Fig. 8(b). According to the pore diameter, the pores can be

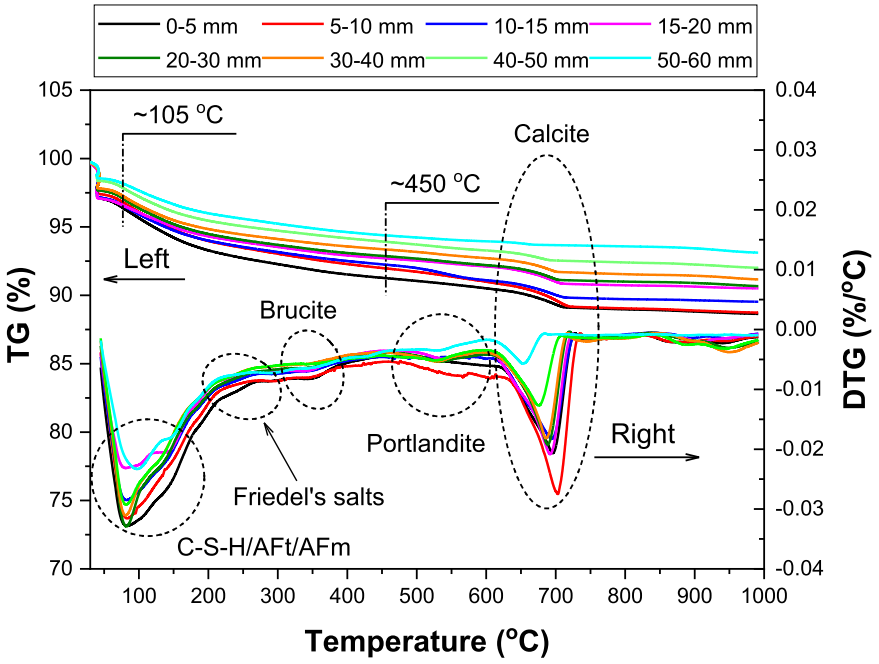

Fig. 7. The TG and DTG patterns of the drilled sample in different layers.

classified into the following three types: small capillary pores (<10 nm), medium capillary pores (10–50 nm), and macro-pores (>50 nm). It can be observed that the total porosity of the sample in the layer of 0–5 mm is relatively higher than that in the layer of 50–60 mm, while the relative percentage of macropores close to the outer layers is larger than that in the inner layers. Moreover, the medium capillary pores in the layer of 0–5 mm are also higher than those in the layer of 50–60 mm, while the small capillary pores are relatively similar in both layers. These results suggest that the presence of various ions in the mining wastewater can react with hydrated phases, leading to the formation of other hydrated products such as AFt, and adversely affecting the microstructure properties of the concrete, which could contribute to an increase in the relative percentage of macropores in the samples close to the erosion surface, as observed in the pore size distribution results. Generally, by comparing the pore size distribution and the porosity of the sample in the different layers, the microstructural performance of the drilled sample can be significantly affected by the presence of various ions in the mining wastewater.

3.3.2. Scanning electron microscopy with energy dispersive spectroscopy (SEM-EDS)

To distinguish the microstructural properties of the drilled cylinder specimen in different layers, the morphologies of the drilled sample near the erosion surface and inner surface were examined and presented in Fig. 9. Referring to Fig. 9(a) to (d), a large amount of randomly distributed calcite can be observed on the microstructural matrices of the sample close to the erosion surface, and the distribution of the determined C-S-H gels is relatively loose in the microstructural matrices. These observations provide further confirmation that the aggressive ions in the mining wastewater can react with the hydrated products in the concrete, such as CH, leading to the formation of calcite and causing a decrease in the microstructural stability of the hydrated gels. As a result, the overall microstructural properties of the concrete are adversely affected. Comparing the morphologies shown in Fig. 9(a) to (d), the microstructural properties of the sample in the inner layers are relatively denser, with more stable hydrated phases detected, including C-S-H gels, AFt, and AFm. Moreover, the interfacial transitional zones (ITZs) between the aggregate and cement matrices in the sample in the inner layers are more coherent than those in the sample close to the erosion surface. The looser microstructure of the concrete sample in the outer layer provides evidence for the larger total porosity found in that layer as determined by MIP analysis, which could further affect the overall durability and performance of the concrete. Additionally, the looser microstructure creates more pathways for aggressive ions to penetrate the concrete, which can lead to further deterioration over time.

Furthermore, SEM-EDS elemental mapping was used to examine the morphology of the drilled concrete samples in different layers, as shown in Fig. 10. The EDS results of ten points determined in the morphologies are also listed in Table 3. Generally, all elements including Si, Al, Ca, O, C, Fe, Mg, Na, Cl, K, and S were detected in both the erosion and inner surface samples in the SEM-EDS mapping results. However, the relative content and distribution of these elements may vary in different layers. It can be observed that the distribution of Al in the Ca-rich zone of the samples close to the erosion surface is relatively lower than that in the inner layers, which confirms the lower peak intensity of AFt and AFm of the sample close to the erosion surface shown in the XRD pattern. The distribution of S is more obvious and widely distributed in the Al-rich zone in the inner surface than in the erosion surface, which indicates that the stability of the hydrated phases with the content of Al and S is relatively higher in the inner layers. However, the wider distribution of K, Cl, and Na in the erosion surface morphologies may indicate that these ions have penetrated deeper into the concrete in that region due to exposure to mining wastewater. In contrast, the lower distribution of these elements in the inner surface morphologies suggests that the ions have not penetrated as deeply into the concrete in those regions. The widely distributed Cl element in the sample close to the erosion surface might also be related to the formation of Friedel's salts and chloride bound in C-S-H gels, which has also been confirmed by other researchers [14,22].

Meanwhile, Table 3 lists the atomic percent of all elements and the ratios of Ca/Si, Al/Ca, and S/Al. The EDS results of the first five points were determined in the erosion surface in an Al-rich and Ca-rich zone, while the remaining results were recorded in the inner layers also enriched in Al and Ca. It can be observed that the atomic percentage of Ca and the ratio of Ca/Si are comparatively lower in

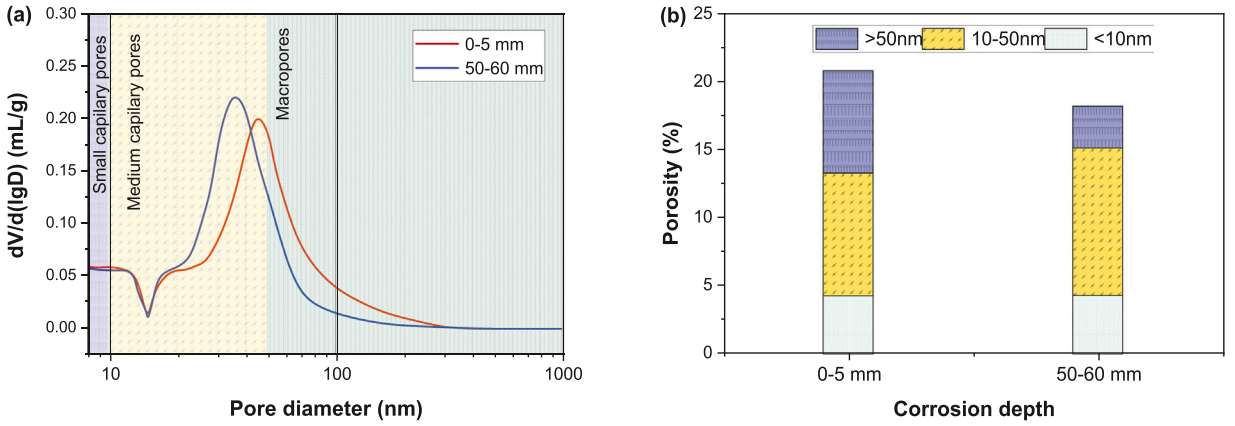

(a) Pore size distribution (b) Pore volume.

Fig. 8. Pore structure of drilled sample in the different layers.

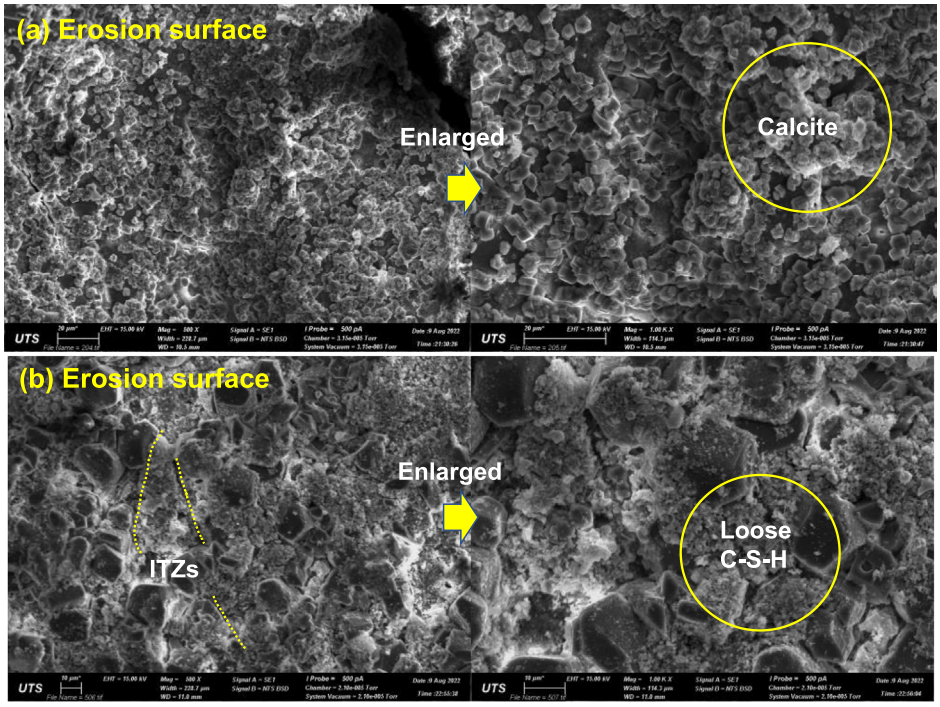

(a) and (b) Erosion surface

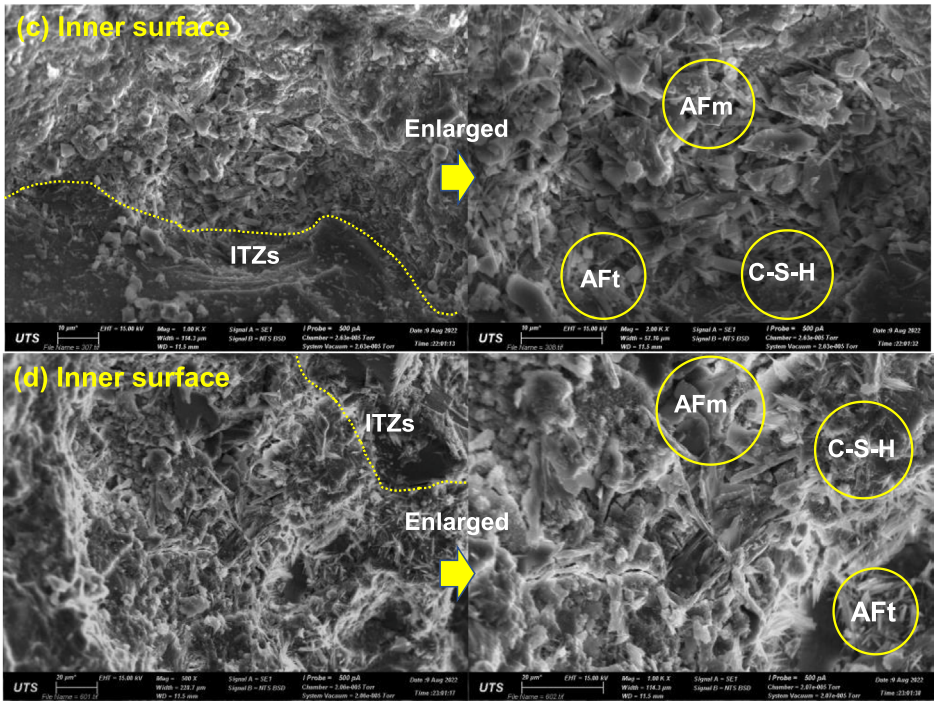

(c) and (d) Inner surface

Fig. 9. Micro morphologies of the drilled concrete exposure to the mining environment for up to 20 years.

the cement matrices close to the erosion surface than those close to the inner surface, while the Al/Ca ratio is relatively higher in the cement matrices in the outer layers than that in the inner layers. This could be related to decalcification, which occurs when Ca leaches out from the cement matrices into the mining wastewater, which also suggests that magnesium ions may play a role in exchanging Ca atoms from hydrated phases such as C-S-H gels [26]. In addition, the atomic percentage of S in the cement matrices close to the erosion

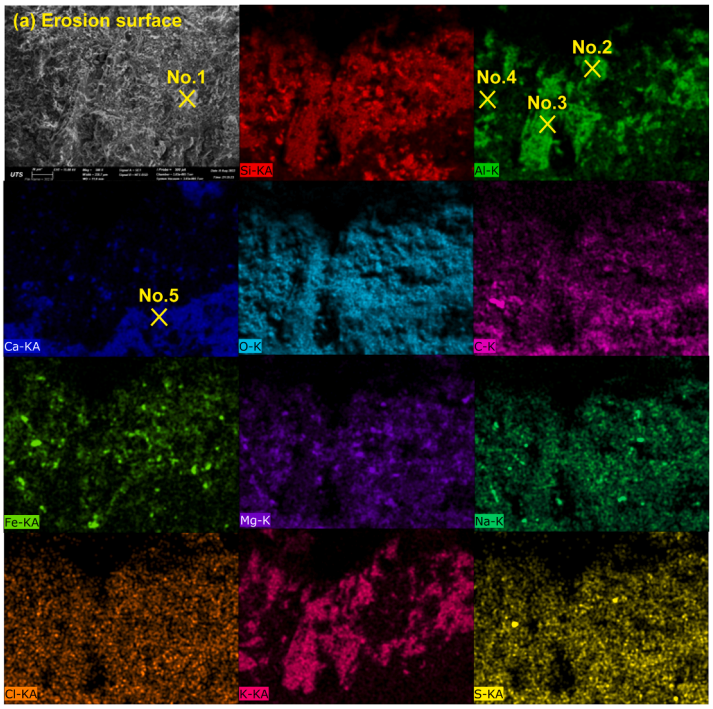

(a) In the erosion

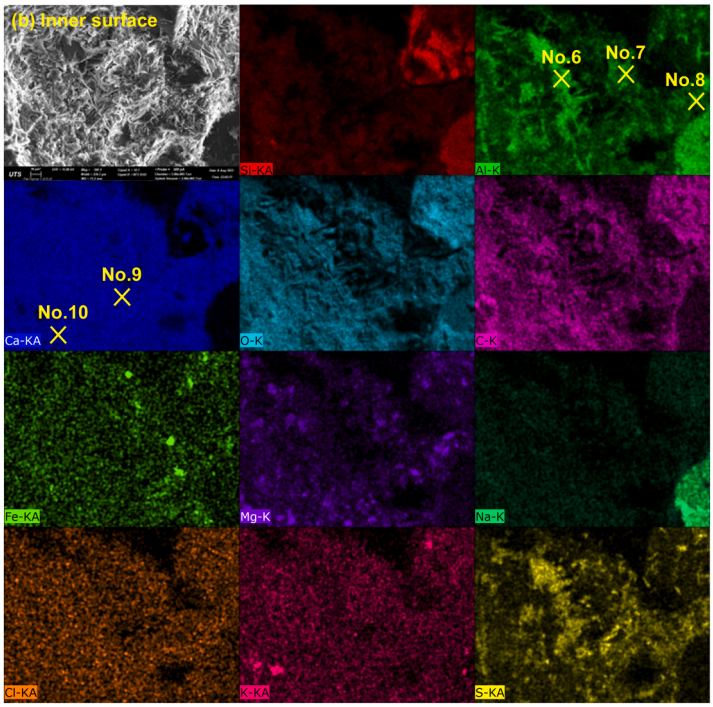

(b) In inner surface

Fig. 10. Micrographs with SEM-EDS elemental mappings of the drilled concrete sample in the erosion and inner surface.

surface is higher than that in the inner layers, while the opposite is found for Cl. This suggests that Cl ions can be bounded to the hydrated phases (C-S-H gels or FS), and the higher Cl content in the mining wastewater can hinder the formation of hydrated phases with a high content of S, especially AFt/AFm, leading to an increased generation of Friedel's salts with a high content of Cl [46]. There is also a lower ratio of S/Al in the cement matrices close to the erosion surface than that in the inner layers, which explains why the

Table 3
EDS results of the drilled concrete samples in different layers.

No.	Elemental atomic percent (%)											Ratios		
	C	O	Na	Mg	Al	Si	S	Cl	K	Ca	Fe	Ca/Si	Al/Ca	S/Al
1	14.95	62.08	0.89	4.40	3.07	10.33	0.06	0.04	0.90	2.08	1.19	0.20	1.48	0.02
2	14.82	31.13	1.15	0.96	0.80	29.68	0.04	0.05	0.31	1.40	19.64	0.05	0.57	0.05
3	10.76	62.09	0.75	0.48	5.44	15.83	0.01	0.01	3.68	0.62	0.33	0.04	8.82	0.00
4	21.25	46.00	0.22	0.90	0.38	14.03	0.00	0.03	3.80	0.49	12.91	0.03	0.77	0.00
5	12.62	64.88	0.59	1.26	3.40	9.07	0.06	0.01	2.05	5.62	0.43	0.62	0.61	0.02
6	7.17	67.93	0.00	0.03	5.53	0.43	2.24	0.00	0.74	15.74	0.20	36.92	0.35	0.41
7	10.20	65.90	0.34	4.53	4.22	2.50	0.59	0.00	0.53	10.02	1.18	4.01	0.42	0.14
8	12.78	66.84	0.25	0.15	2.76	1.99	1.33	0.00	0.59	12.96	0.35	6.51	0.21	0.48
9	0.00	22.26	0.01	0.00	1.30	1.24	2.45	0.00	3.17	67.81	1.75	54.51	0.02	1.88
10	11.64	68.85	0.46	3.79	2.87	4.16	0.08	0.00	0.04	8.01	0.11	1.93	0.36	0.03

intensity peak of AFt and AFm is relatively lower in outer layers than in inner layers, as shown in the XRD results mentioned in Section 3.2.1.

4. Conclusions

In this study, the combined effects of the various ions present in the mining wastewater on the phase transformation of the concrete were evaluated based on a drilled cylinder concrete specimen from a field concrete dam, which has been under-used for the temporary storage of mining wastewater in Western Australia for over 20 years. Various analysis methods were employed to analyze the microstructural properties and chemical reactions between the hydrated phases and the various ions in the mining environment. Based on the results, some conclusions are shown as follows:

(1) The chemical and mineralogical properties of the cement matrices in the outer layers of the concrete dam have been significantly affected by long-term exposure to mining wastewater. The performance of the concrete dam can be influenced not only by the various ions (such as magnesium, sulfate, and chloride ions) in the mining wastewater, but also by external factors, such as atmospheric carbonate content.
(2) Carbonation is a common form of attack on concrete structures in mining environments. The XRD, FTIR, and TGA results confirmed the presence of calcite as the carbonate phase resulting from the chemical reaction between portlandite and carbonate ions. This reaction was detected in both outer layers (0–5 mm) and inner layers (50–60 mm), indicating that carbonation can occur throughout the drilled cylinder specimens from the concrete dam.
(3) The concrete dam in the mining environment is susceptible to sulfate attacks, especially on the erosion surface, due to the high concentration of sulfate ions in the wastewater, which can lead to the generation of aluminate-rich hydrated products. The experimental results indicated that the relative intensity of the AFt and AFm peaks (XRD results) in the outer layers of the drilled cylinder specimen from the concrete dam was lower than that in the inner layers, which might be related to the high Cl content in the mining wastewater, leading much more AFt/AFm being transformed into Friedel's salts. The Mg ions in the mining wastewater might have a positive effect on exchanging the Ca atomic from the hydrated phases, such as C-S-H gels, in the cement matrices, which could increase the decalcification process.
(4) The various ions present in mining wastewater can lead to transformations of the hydrated phases and further affect the microstructural performance of concrete structures. The MIP test confirmed that the total porosity and microporosity of the sample near the erosion surface were higher than those in the inner layers. The SEM-EDS analysis also confirmed that the ITZs between the aggregate and cement matrices were relatively stable in the non-degraded area. Besides, the SEM-EDS mapping results showed that the distribution and relative content of various elements, such as Al, Ca, S, K, Na, and Cl, were different in the outer and inner layers of the concrete dam, which indicated the combined effects of various ions in the mining wastewater on the phase transformation of the concrete.
(5) The comprehensive analysis results demonstrated that the mining wastewater had a significant impact on the microstructural and chemical properties of the concrete dam, which highlights the importance of regular monitoring and maintenance for concrete structures in mining environments. In addition, the effects of other environmental conditions, like water pressure or weather changes, the performance of dam concrete will be further investigated to ensure the safety of the concrete structure.

Declaration of Competing Interest

The authors declare that they have no known competing financial interests or personal relationships that could have appeared to influence the work reported in this paper.

Data Availability

Data will be made available on request.

Acknowledgments

The authors gratefully acknowledge the support from the Innovation Connections project between YAT Engineering and Construction and the Australian Department of Industry, Innovation and Science (ICG002073).

References

[1] I. Arribas, I. Vegas, V. García, R.V. De La Villa, S. Martínez-Ramírez, M. Frías, The deterioration and environmental impact of binary cements containing thermally activated coal mining waste due to calcium leaching, J. Clean. Prod. 183 (2018) 887–897.
[2] F. Bellmann, W. Erfurt, H.-M. Ludwig, Field performance of concrete exposed to sulphate and low pH conditions from natural and industrial sources, Cem. Concr. Compos. 34 (1) (2012) 86–93.
[3] D. Sun, Z. Cao, C. Huang, K. Wu, G. De Schutter, L. Zhang, Degradation of concrete in marine environment under coupled chloride and sulfate attack: a numerical and experimental study, Case Stud. Constr. Mater. 17 (2022), e01218.
[4] F. Qu, W. Li, W. Dong, V.W. Tam, T. Yu, Durability deterioration of concrete under marine environment from material to structure: a critical review, J. Build. Eng. 35 (2021), 102074.
[5] A. Strazzabosco, J.H. Gruenhagen, S. Cox, A review of renewable energy practices in the Australian mining industry, Renew. Energy (2022).
[6] C. Tiemann, V. MacDonald, R. Young, K. Dixon, Rehabilitation and mine closure policies creating a pathway to relinquishment: an Australian perspective, Restor. Ecol. 30 (2022), e13785.
[7] L. Caneda-Martínez, W. Kunther, C. Medina, M.I.S. de Rojas, M. Frías, Exploring sulphate resistance of coal mining waste blended cements through experiments and thermodynamic modelling, Cem. Concr. Compos. 121 (2021), 104086.
[8] C. Wang, J. Xiao, C. Long, Q. Zhang, J. Shi, Z. Zhang, Influences of the joint action of sulfate erosion and cementitious capillary crystalline waterproofing materials on the hydration products and properties of cement-based materials: a review, J. Build. Eng. (2023), 106061.
[9] L. Qin, X. Mao, X. Gao, P. Zhang, T. Chen, Q. Li, Y. Cui, Performance degradation of CO_2 cured cement-coal gangue pastes with low-temperature sulfate solution immersion, Case Stud. Constr. Mater. 17 (2022), e01199.
[10] T.H. Vu, L.C. Dang, G. Kang, V. Sirivivatnanon, Chloride induced corrosion of steel reinforcement in alkali activated concretes: a critical review, Case Stud. Constr. Mater. (2022), e01112.
[11] A. Saedi, A. Jamshidi-Zanjani, M. Mohseni, A.K. Darban, Effect of mechanochemical activation on hydration properties of lead-zinc sulfide tailings for concrete construction, Case Stud. Constr. Mater. 18 (2023), e01996.
[12] G. Deng, Y. He, L. Lu, F. Wang, S. Hu, Investigation of sulfate attack on aluminum phases in cement-metakaolin paste, J. Build. Eng. 56 (2022), 104720.
[13] L.G. Baquerizo, T. Matschei, K.L. Scrivener, M. Saeidpour, L. Wadsö, Hydration states of AFm cement phases, Cem. Concr. Res. 73 (2015) 143–157.
[14] K. De Weerdt, E. Bernard, W. Kunther, M.T. Pedersen, B. Lothenbach, Phase changes in cementitious materials exposed to saline solutions, Cem. Concr. Res. 165 (2023), 107071.
[15] A. Saedi, A. Jamshidi-Zanjani, A.K. Darban, M. Mohseni, H. Nejati, Utilization of lead–zinc mine tailings as cement substitutes in concrete construction: effect of sulfide content, J. Build. Eng. 57 (2022), 104865.
[16] E. Rozière, A. Loukili, R. El Hachem, F. Grondin, Durability of concrete exposed to leaching and external sulphate attacks, Cem. Concr. Res. 39 (12) (2009) 1188–1198.
[17] E. Gruyaert, P. Van den Heede, M. Maes, N. De, Belie, Investigation of the influence of blast-furnace slag on the resistance of concrete against organic acid or sulphate attack by means of accelerated degradation tests, Cem. Concr. Res. 42 (1) (2012) 173–185.
[18] Z. Chen, J. Yu, V. Bindiganavile, C. Yi, C. Shi, X. Hu, Time and spatially dependent transient competitive antagonism during the 2-D diffusion-reaction of combined chloride-sulphate attack upon concrete, Cem. Concr. Res. 154 (2022), 106724.
[19] G. Paul, E. Boccaleri, L. Buzzi, F. Canonico, D. Gastaldi, Friedel's salt formation in sulfoaluminate cements: a combined XRD and 27Al MAS NMR study, Cem. Concr. Res. 67 (2015) 93–102.
[20] F. Qu, W. Li, Y. Guo, S. Zhang, J.L. Zhou, K. Wang, Chloride-binding capacity of cement-GGBFS-nanosilica composites under seawater chloride-rich environment, Constr. Build. Mater. 342 (2022), 127890.
[21] P. Li, W. Li, T. Yu, F. Qu, V.W. Tam, Investigation on early-age hydration, mechanical properties and microstructure of seawater sea sand cement mortar, Constr. Build. Mater. 249 (2020), 118776.
[22] K. De Weerdt, H. Justnes, M.R. Geiker, Changes in the phase assemblage of concrete exposed to sea water, Cem. Concr. Compos. 47 (2014) 53–63.
[23] K. De Weerdt, H. Justnes, The effect of sea water on the phase assemblage of hydrated cement paste, Cem. Concr. Compos. 55 (2015) 215–222.
[24] K. De Weerdt, B. Lothenbach, M.R. Geiker, Comparing chloride ingress from seawater and NaCl solution in Portland cement mortar, Cem. Concr. Res. 115 (2019) 80–89.
[25] X. Shi, N. Xie, K. Fortune, J. Gong, Durability of steel reinforced concrete in chloride environments: an overview, Constr. Build. Mater. 30 (2012) 125–138.
[26] S. Cheng, Z. Shui, T. Sun, X. Gao, C. Guo, Effects of sulfate and magnesium ion on the chloride transportation behavior and binding capacity of Portland cement mortar, Constr. Build. Mater. 204 (2019) 265–275.
[27] S.R. Pinto, C.A. da Luz, G.S. Munhoz, R.A. Medeiros-Junior, Durability of phosphogypsum-based supersulfated cement mortar against external attack by sodium and magnesium sulfate, Cem. Concr. Res. 136 (2020), 106172.
[28] A. Skaropoulou, S. Tsivilis, G. Kakali, J. Sharp, R. Swamy, Long term behavior of Portland limestone cement mortars exposed to magnesium sulfate attack, Cem. Concr. Compos. 31 (9) (2009) 628–636.
[29] S. Zhou, H. Lv, Y. Wu, Degradation behavior of concrete under corrosive coal mine environment, Int. J. Min. Sci. Technol. 29 (2) (2019) 307–312.
[30] K. De Weerdt, G. Plusquellec, A.B. Revert, M. Geiker, B. Lothenbach, Effect of carbonation on the pore solution of mortar, Cem. Concr. Res. 118 (2019) 38–56.
[31] D. Anstice, C. Page, M. Page, The pore solution phase of carbonated cement pastes, Cem. Concr. Res. 35 (2) (2005) 377–383.
[32] W. Ashraf, Carbonation of cement-based materials: challenges and opportunities, Constr. Build. Mater. 120 (2016) 558–570.
[33] T. Sibbick, D. Fenn, N. Crammond, The occurrence of thaumasite as a product of seawater attack, Cem. Concr. Compos. 25 (8) (2003) 1059–1066.
[34] M. Rahman, M. Bassuoni, Thaumasite sulfate attack on concrete: mechanisms, influential factors and mitigation, Constr. Build. Mater. 73 (2014) 652–662.
[35] A. Skaropoulou, K. Sotiriadis, G. Kakali, S. Tsivilis, Use of mineral admixtures to improve the resistance of limestone cement concrete against thaumasite form of sulfate attack, Cem. Concr. Compos. 37 (2013) 267–275.
[36] L. Lin, B. Wu, Water permeability behavior of recycled lump/aggregate concrete, Constr. Build. Mater. 323 (2022), 126508.
[37] Y. Yi, D. Zhu, S. Guo, Z. Zhang, C. Shi, A review on the deterioration and approaches to enhance the durability of concrete in the marine environment, Cem. Concr. Compos. 113 (2020), 103695.
[38] L. Zhou, V. Sarfarazi, H. Haeri, A.A. Naderi, M.F. Marji, F. Wu, Study on shear fracture behavior of soft filling in concrete specimens: experimental tests and numerical simulation, Struct. Eng. Mech. 85 (3) (2023) 337–351.
[39] A. Bagher Shemirani, H. Haeri, V. Sarfarazi, P. Ebneabbasi, M.Fatehi Marji, Investigation of the interaction between concrete-gypsum interface and internal notch using experimental test and numerical simulation, Mech. Based Des. Struct. Mach. (2020) 1–24.
[40] S. Abharian, V. Sarfarazi, M.F. Marji, H. Rasekh, A. Sadrekarimi, Effect of geogrid reinforcement on tensile failure of high-strength self-compacted concrete, Mag. Concr. Res. 75 (8) (2023) 379–401.
[41] Y. Wang, Y. Cao, P. Zhang, Y. Ma, T. Zhao, H. Wang, Z. Zhang, Water absorption and chloride diffusivity of concrete under the coupling effect of uniaxial compressive load and freeze–thaw cycles, Constr. Build. Mater. 209 (2019) 566–576.

[42] P. Zhang, F.H. Wittmann, M. Vogel, H.S. Müller, T. Zhao, Influence of freeze-thaw cycles on capillary absorption and chloride penetration into concrete, Cem. Concr. Res. 100 (2017) 60–67.
[43] T. Missana, M. García-Gutiérrez, M. Mingarro, U. Alonso, Comparison between cesium and sodium retention on calcium silicate hydrate (CSH) phases, Appl. Geochem. 98 (2018) 36–44.
[44] K. De Weerdt, D. Orsáková, M.R. Geiker, The impact of sulphate and magnesium on chloride binding in Portland cement paste, Cem. Concr. Res. 65 (2014) 30–40.
[45] K. De Weerdt, D. Orsáková, A.C. Müller, C.K. Larsen, B. Pedersen, M.R. Geiker, Towards the understanding of chloride profiles in marine exposed concrete, impact of leaching and moisture content, Constr. Build. Mater. 120 (2016) 418–431.
[46] A. Machner, M. Zajac, M.B. Haha, K.O. Kjellsen, M.R. Geiker, K. De Weerdt, Stability of the hydrate phase assemblage in Portland composite cements containing dolomite and metakaolin after leaching, carbonation, and chloride exposure, Cem. Concr. Compos. 89 (2018) 89–106.